The Open Construction and Building Technology Journal

Content list available at: https://openconstructionandbuildingtechnologyjournal.com

RESEARCH ARTICLE

An Enhanced Beam Model for the Analysis of Masonry Walls

Massimiliano Lucchesi[1], Barbara Pintucchi[1,*] and Nicola Zani[1]

[1]*Department of Civil and Environmental Engineering (DICeA), University of Florence, Piazza Brunelleschi 6, 50121 Florence, Italy*

Abstract:

Background:

Some typologies of masonry constructions (*e.g.* towers or walls with openings) can be reasonably studied through simple beam or frame-like models. For these structures, shear mechanisms often play an important role inducing failure and collapse.

Objective:

The paper presents an enriched beam model for studying the in-plane response of masonry walls. Initially formulated for masonry columns, towers and masonry slender structures in general, the model is now modified in order to also capture the shear failure mechanisms, in addition to the flexural ones.

Methods:

Starting with a one-dimensional no-tension model, a strength domain in the plane of the axial and tangential stress of the beam has been added, which has been defined by limiting both the stress shear component with respect to any possible direction and the main compressive stress.

Results:

The model, implemented in the FEM computational code MADY, allows for short computational times in studying the response of single panels as well as walls with openings.

Conclusion:

Comparisons of some experimental results from literature and some numerical results from more refined 2D models show the effectiveness and accuracy of the model's predictions in terms of global and local response.

Keywords: Masonry, Panels, Nonlinear, Finite elements, Beam model, Equivalent frame, In-plane behaviour.

Article History	Received: November 29, 2018	Revised: January 23, 2019	Accepted: February 17, 2019

1. INTRODUCTION

The issue of modelling masonry structures is still an open one in structural engineering. This is due to the complexity of the material's mechanical behaviour together with the great variety of structural types and constituents, that is mortar and bricks, and their textures. Meanwhile, seismic assessment, repair and strengthening of ancient masonry buildings is a priority, as such structures represent a large part of the cultural heritage of the Mediterranean basin. In particular, masonry's lateral load capacity is crucial in seismic areas, where old masonry buildings have often exhibited high vulnerability to earthquakes.

* Address correspondence to this author at the Department of Civil and Environmental Engineering (DICeA), University of Florence, Piazza Brunelleschi 6, 50121 Florence, Italy; Tel: +390552756850;
E-mail: barbara.pintucchi@unifi.it

Within this framework, nonlinear static procedures and equivalent-frame models have become very popular and attractive for practical engineering applications. The increasingly relevant role played by nonlinear static analyses in recent decades, and the widespread use of equivalent-frame models for studying ordinary masonry buildings stem from a common reason: the advantage of accounting for nonlinear structural behaviour, while preserving relative simplicity and modest computational costs.

Substantially, in the equivalent-frame approach, a masonry wall with rather regularly spaced openings can be idealized as composed of a series of panels - distinguished into piers and spandrels - connected by rigid nodes, whose dimensions can be defined through the alignments of the openings and/or the "effective" heights of the piers revealed by the damage patterns occurring under earthquakes and codified by the relevant

literature [1, 2]. A thorough discussion concerning the features and benefits of using such models in comparison with others can be found in a few studies [3 - 5].

A large number of models following the equivalent-frame method have been proposed in the literature over the last decade [6 - 10]. Most of these make use of macro-elements to represent piers and spandrels. Often, they are developed assuming the classical hypotheses of a beam and make use of a limited number of nodes. Furthermore, they generally rely on a phenomenological description of the constitutive behavior of the panel, especially for shear resistance behavior. The Interested readers may refer to another study [11] for a comprehensive state-of-the-art review.

This paper presents an advanced one-dimensional continuum model for non-linear static analysis of masonry shear walls.

In the previous research by the authors, a numerical model was defined, which performed non-linear static and dynamic analyses on masonry columns, arches, towers, and slender structures in general. The model relies on a costitutive equation formulated in terms of generalized strain and stress for beams with various cross-sections, under the hypotheses that the material is non-linear elastic, unable to withstand tension with limited compressive strength [12, 14]. Furthermore, to describe the cyclical behavior and seismic response of masonry elements more realistically, a damage process under compression has been introduced [15]. The model has been implemented in the FEM computational code MADY and applied to the study of several slender masonry structures, which typically exhibit flexural behavior and consequent failure mechanism [16, 17].

Indeed, in the past one-dimensional no-tension models have been used extensively to study problems of the stability of masonry columns [18 - 20], the static and dynamic response of unreinforced and reinforced arches and vaults [21 - 23], as well as the out-of-plane behavior of masonry panels and walls. The same does not hold for the study of the in-plane behavior of masonry panels under lateral actions. In this case, as is widely known, panels are likely to undergo various distinct failure mechanisms, or a combination of some of them: for flexural behaviour (rocking/toe-crushing failure), as well as for shear with diagonal cracking or sliding along bed-joints [3, 24], which cannot be modelled using classical no-tension beam models.

The proposed constitutive model has been enhanced to address shear behaviour and account for failure with diagonal cracking in masonry panels. To this aim, the beam is formulated according to the Timoshenko theory to account for shear deformations; then, a constitutive law is defined for the shear force, in addition to that proposed for the axial one and bending moment.

Essentially, the constitutive model is characterized by a strength domain in the plane of the axial and tangential stresses of the beam, which has been defined by limiting the stress shear component with respect to any possible plane of the panel; namely, not only with respect to the one orthogonal to the beam axis. Furthermore, in analogy to the proposal for the shear stress, the principal compressive stress, rather than the axial stress component of the beam, has been limited to achieving maximum strength.

In the following, the proposed model is first presented, and then some numerical results are provided and compared to some experimental data available in the literature.

Then, some numerical analyses are conducted in order to highlight the potential of the model to approximate the 2D solution. To this end, some results obtained through the proposed models are compared with those obtained *via* the commercial code ANSYS [25] and *via* the formulated bi-dimensional masonry-like model [26].

Lasly, preliminary results on an idealized wall with a centered opening are provided as an example for practical applications.

2. MODEL SPECIFICATIONS

In order to introduce a constitutive equation also for shear behaviour, in addition to axial/flexural one, shear deformations are accounted for according to the Timoshenko theory (see Section 2.1).

Then, a nonlinear-elastic constitutive model is assumed for describing masonry's response. Specifically, a strength domain in the plane of the stress components of a 2D beam (σ_z-τ_{zy}) has been defined, as explained in detail in Section 6.

Given the kinematic constrains and the material constitutive laws, the patterns of the axial stress σ_z and the tangential stress τ_{zy} over the beam's cross-section can thus be determined for any strain pattern, as shown by the examples provided in Section 8. Finally, by simply integrating these stresses, a constitutive relation which associates the generalized stresses axial force N, shear V and bending moment M- to the generalized strains - ε, κ and γ- has been obtained.

2.1. Kinematic Hypothesis

According to the Timoshenko beam theory, cross-sections remain plane after bending but not necessarily normal to the deformed axis of the beam. Hence, the displacement field is identified through the longitudinal and transverse displacements of the beam's axis, u, v and the rotation of the cross-section φ, which is independent of v.

The total slope of the deflected beam's axis is due to both bending and shear, and is given by:

$$\frac{dv}{dz} = \varphi - \gamma \qquad \textbf{(1)}$$

where z denotes the abscissa along the beam axis and γ is the transverse shear strain. Overall, the generalized strains are given by:

$$\varepsilon = u', \gamma = \varphi - v', \kappa = \varphi' \qquad \textbf{(2)}$$

where ε is the extensional strain and κ the curvature of the beam axis.

Lastly, it is worth noting that, in view of the hypothesis of plane sections, each longitudinal fiber undergoes the axial strain:

$$\varepsilon_z = \varepsilon + \kappa y \qquad \textbf{(3)}$$

where y is the distance between the fiber and the geometrical centre of the cross-section.

2.2. Constitutive Models and Definition of the Strength Domain σ_z-τ_{zy}

With reference to the coordinate system shown in Fig. (**1**), let's assume that the stress state at any point of any beam's cross section is completely described by the components σ_z (axial stress) and τ_{zy} (tangential stress). The formulation of the model stems from the idea of defining a strength domain σ_z-τ_{zy} while keeping in mind a plane state of stress, where σ_y is supposed to be nil ($\sigma_y = 0$).

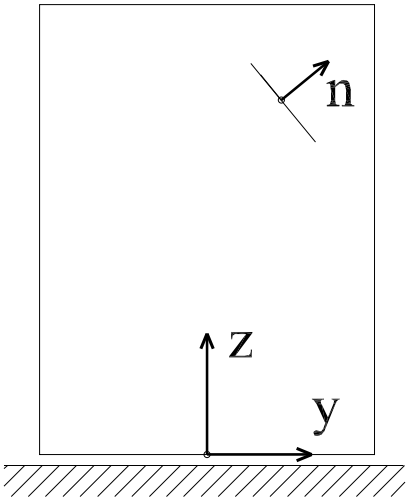

Fig. (1). Sketch of the panel and reference system.

In particular, the beam's strength domain σ_z-τ_{zy} has been defined by requiring some conditions on the stress to be satisfied. As widely used in the framework of no-tension beam models [27], the material does not withstand traction in the z-direction, *i.e.* σ_z is assumed to be non-positive. Moreover, with reference to a plane state of stress, the new condition assumed herein -referred to in the following as Condition (1)- requires that, at any point of the panel, the shear stress component τ_n on any plane - defined by its normal direction **n** (Fig. **1**)- must respect the Mohr-Coulomb criterion, that is:

$$|\tau_n| \le \tau_o + m\sigma_n \qquad \forall \mathbf{n} \qquad \textbf{(4)}$$

where σ_n denotes the normal stress component parallel to **n**, and $\tau_o > 0$ and $m < 0$ are two constant material parameters, usually known as cohesion and internal friction, respectively.

With reference to the plane (σ, τ), the foregoing condition corresponds to requiring that any state of stress in the panel, which can be represented graphically through the Mohr circle, will be admissible if it is internal to the cone with vertex at point ($-\tau_o/m$,0) and identified by the half-lines $\tau = \pm(\tau_o + m\sigma)$. Hence, by requiring that the circle be tangent to these two half-lines (Fig. **2**), it is a simple matter to verify that Eq. (4) can also be written as

$$\sigma^+(\sqrt{1+m^2} - m) - \sigma^-(\sqrt{1+m^2} + m) \le 2\tau_o, \qquad \textbf{(5)}$$

where σ^- and σ^+ denote the principal stresses.

The second condition *i.e.* Condition (2) consists of assuming that the minimum negative normal stress (compression) on any plane is greater than the minimum admissible compressive stress τ, namely

$$\sigma^- \ge \sigma_o. \qquad \textbf{(6)}$$

Referring to the reference system (o,y,z) depicted in Fig. (**1**), where the z-direction corresponds to the beam's longitudinal axis, let's assume that the plane stress state in the panel is

$$\mathbf{T} = \begin{bmatrix} 0 & \tau_{zy} \\ \tau_{zy} & \sigma_z \end{bmatrix} \qquad \textbf{(7)}$$

where σ_y is assumed to be negligible (quite an acceptable hypothesis especially for modest stress states [3]).

Consequently, the principal stresses turn out to be

$$\sigma^- = \frac{\sigma_z}{2} - \frac{1}{2}\sqrt{{\sigma_z}^2 + 4{\tau_{zy}}^2} \qquad \textbf{(8)}$$

$$\sigma^+ = \frac{\sigma_z}{2} + \frac{1}{2}\sqrt{{\sigma_z}^2 + 4{\tau_{zy}}^2}.$$

and the domains D_1 and D_2 that respectively guarantee fulfillment of Conditions (1) and (2) can be defined in the plane (σ_z, τ_{zy}).

Specifically, by substituting Eq. (8) into Eq. (5), the domain D_1 shown in Fig. (**3**) has been obtained. Its boundary is the ellipse defined by the equation

$${\sigma_z}^2 + 4(1+m^2){\tau_{zy}}^2 - 4m\tau_o\sigma_z - 4{\tau_o}^2 = 0 \qquad \textbf{(9)}$$

with center at point ($2m\tau_{zy}$, 0) and half minor and major axis respectively equal to τ_o and $2\tau_o\sqrt{1+m^2}$ (Fig. **3**). The ellipse intersects the reference σ_z-axis at the points

$$(2\tau_o(m \mp \sqrt{1+m^2}),0) \qquad \textbf{(10)}$$

and the τ_{zy}-axis at the points

$$(0, \pm\frac{\tau_o}{\sqrt{1+m^2}}). \qquad \textbf{(11)}$$

As per the condition given on σ_z (*i.e.* $\sigma_z \le 0$), the domain of interest is limited to the portion in the half-plane of the negative σ_z (hatched area in Fig. **3**).

Referring to Condition (*2*), domain D_2 is defined by substituting Eq. (8) into Eq. (6), (Fig. **4**). It is limited by the parabola with equation

$${\tau_{zy}}^2 - \sigma_o(\sigma_o - \sigma_z) = 0 \qquad \textbf{(12)}$$

with axis of symmetry coincident with the σ_z-axis, vertex at point (σ_o,0) and intersecting the τ_{zy}-axis at points (0,$\pm\sigma_o$). Also in this case the domain is limited to the portion belonging to the half-plane of negative σ_z (Fig. **4**).

Obviously, simultaneous fulfillment of both Conditions (1) and (2) is guaranteed if the components of stress (σ_z, τ_{zy}) belong

to the intersection $\mathcal{D} = \mathcal{D}_1 \cap \mathcal{D}_2$. In principle, two situations can occurr: if $\sigma_o \leq 2\tau_o(m - \sqrt{1+m^2})$, the intersection of the domains D coincides with D_1 as shown in Fig. (**5a**) where $2\tau_o(m - \sqrt{1+m^2})$

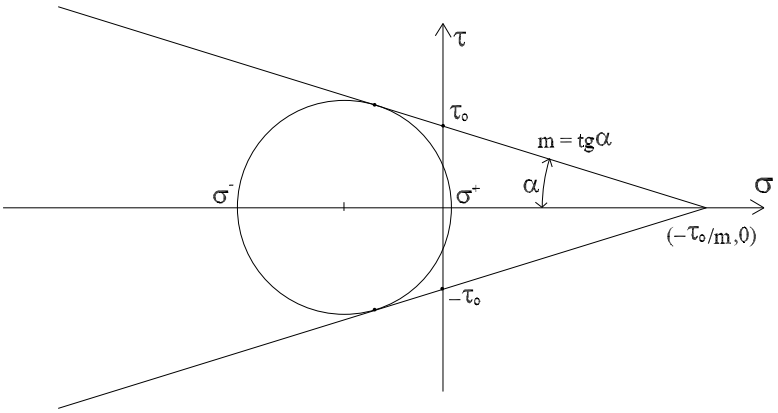

Fig. (2). Assumed stress state.

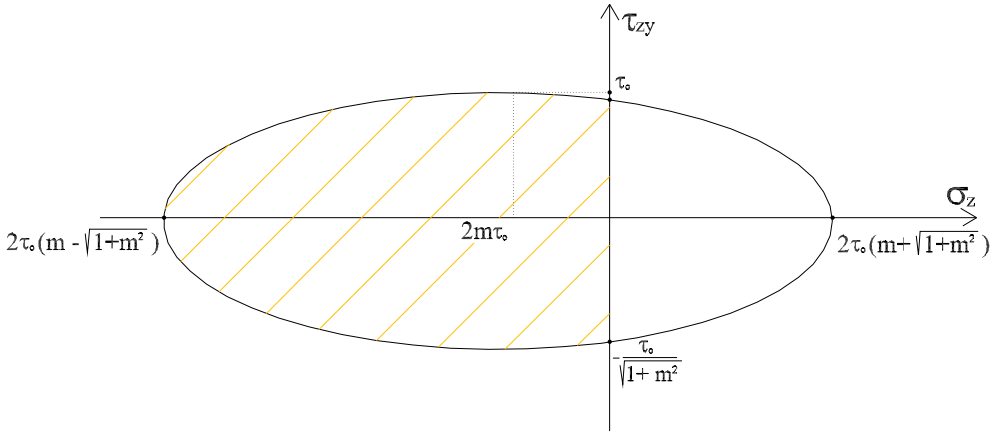

Fig. (3). Strength domain in the plane (σ_z, τ_{zy}), defined by Condition (1).

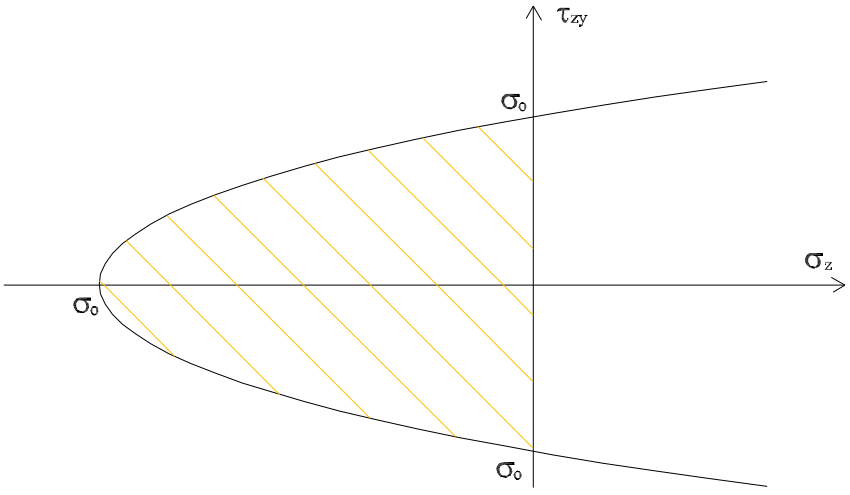

Fig. (4). Strength domain in the plane (σ_z, τ_{zy}), defined by Condition (2).

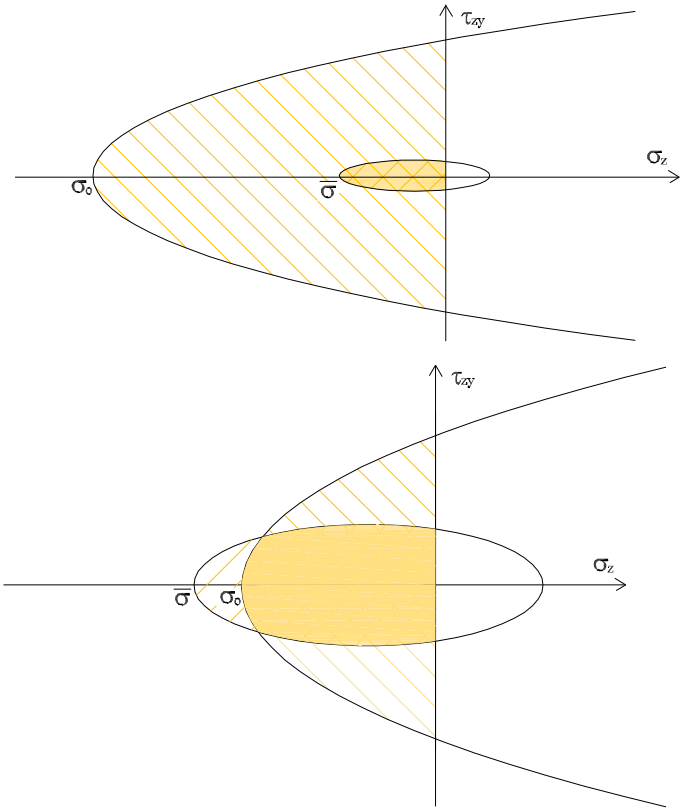

Fig. (5). Possible intersection $\mathcal{D}$ of the two domains $\mathcal{D}_1$ and $\mathcal{D}_2$: a) if $\sigma_o \leq \bar{\sigma}$ and b) if $\sigma_o > \bar{\sigma}$, with $\bar{\sigma} = 2\tau_o(m - \sqrt{1+m^2})$.

has been denoted with $\bar{\sigma}$; in this case, fulfillment of Condition (1) also ensures Condition (2). Conversely, if $\sigma_o > 2\tau_o\sqrt{1+m^2} = \bar{\sigma}$, then $\mathcal{D}$ turns out to be the one depicted in Fig. (**5b**). However, the first situation is of greater interest in practical applications, as it is more likely to occur for the usual values of parameters σ_o, τ_o, and m. Hence, hereafter we always refer to such case, *i.e.* $\mathcal{D} \equiv \mathcal{D}_1$.

It is worth emphasizing that the strength domain $\mathcal{D}$ differs substantially from the one obtained by applying the Mohr-Coulomb criterion solely to the shear stress τ_{zy} acting on the panel's horizontal planes, *i.e.* on the beam's cross-section. In other words, the proposed model differs greatly from that accounting only for horizontal bed joint sliding. Fig. (**6**) shows a comparison.

According to the strength domain assumed and, as already stated, referring to the case $\mathcal{D} \equiv \mathcal{D}_1$ for the sake of simplicity, the constitutive equation can be written as follows:

$$\sigma_z = \begin{cases} 0 & \text{if} \quad \varepsilon_z > 0 \\ E\varepsilon_z & \text{if} \quad \bar{\varepsilon} \leq \varepsilon_z \leq 0 \\ \bar{\sigma} & \text{if} \quad \varepsilon_z \leq \bar{\varepsilon} \end{cases} \qquad \textbf{(13)}$$

with $\bar{\varepsilon} = \bar{\sigma}/E$ and E the Young's modulus; moreover, let

$$\bar{\tau}_{zy} = \frac{1}{2}\sqrt{\frac{4{\tau_o}^2 + 4m\sigma_z\tau_o - {\sigma_z}^2}{1+m^2}} \qquad \textbf{(14)}$$

so that Eq. (9) can be written as $\tau_{zy} = \pm\bar{\tau}_{zy}$, and denoting

$$\bar{\gamma}_{zy} = \frac{\bar{\tau}_{zy}}{G} \qquad \textbf{(15)}$$

with G the shear modulus, the constitutive law for the tangential stress turns out to be

$$\tau_{zy} = \begin{cases} 0 & \text{if} \quad \varepsilon_z \geq 0 \\ G\gamma_{zy} & \text{if} \quad \varepsilon_z < 0 \quad \text{and} \quad |\gamma_{zy}| \leq \bar{\gamma}_{zy} \\ \bar{\tau}_{zy} sign(\gamma_{zy}) & \text{if} \quad \varepsilon_z < 0 \quad \text{and} \quad |\gamma_{zy}| > \bar{\gamma}_{zy}. \end{cases} \qquad \textbf{(16)}$$

3. BEHAVIOR OF THE BEAM'S CROSS SECTION

Given the kinematic assumptions set forth in Section 2.1 and the assumed constitutive law, the normal stress σ_z has a piecewise linear diagram over any rectangular cross section and can be determined. Various possible σ_z patterns can occur, each of which corresponds to a different region in the plane of the generalized strains (ε, κ).

This constitutive equation has been presented in details in [16] for the simpler case in which the effects of shear deformation can be neglected and is not provided herein for the sake of brevity.

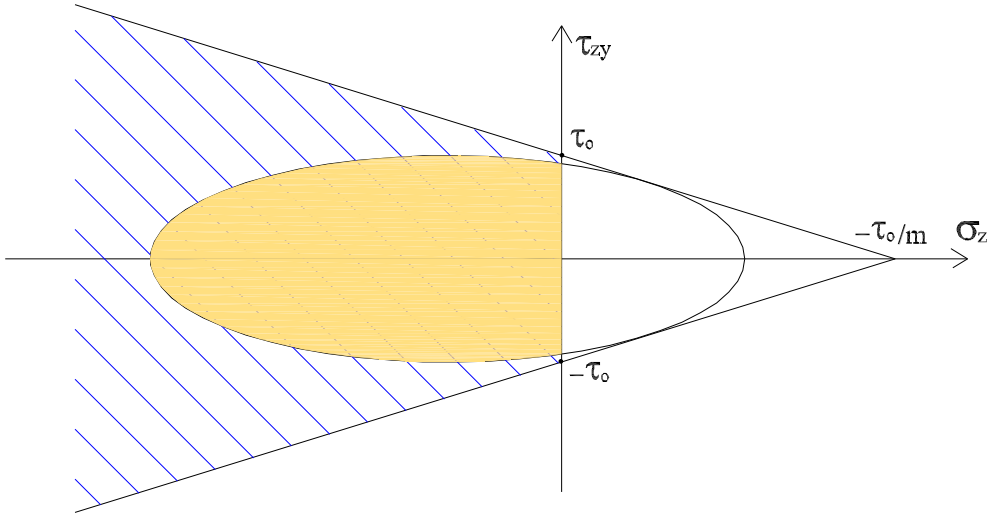

Fig. (6). Comparison of the proposed domain with the case of Mohr-Coulomb failure only on bed joint layers.

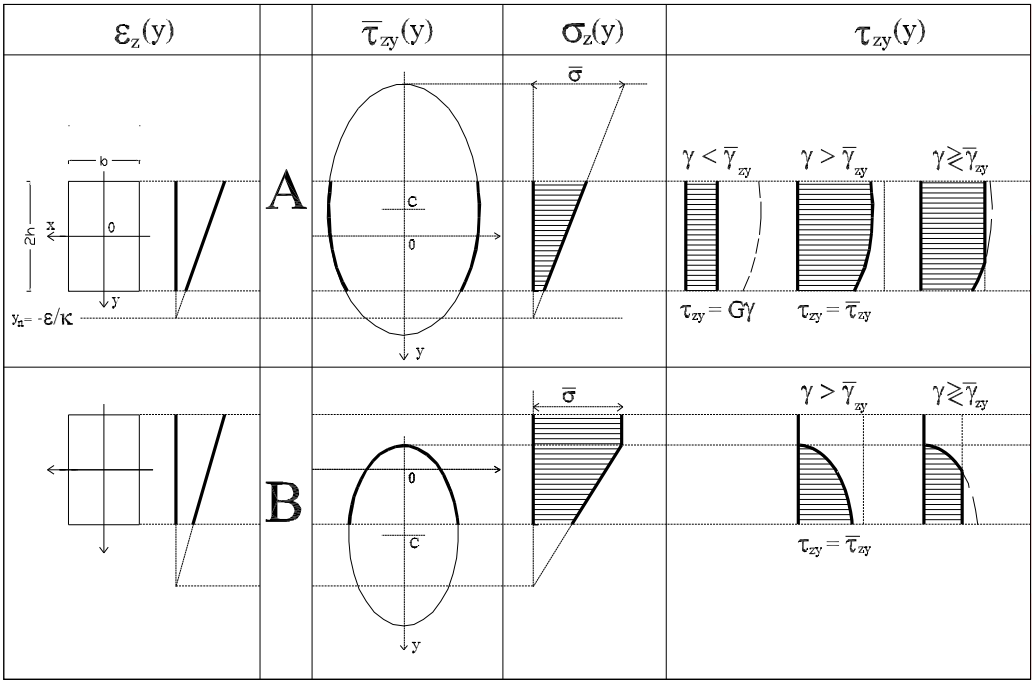

Fig. (7). σ_z and τ_{zy} patterns over a non-partialized beam cross-section.

As regards the τ_{zy} patterns, some clarification is in order. It is firstly worth noting that, once the values of the parameters τ_o and m are fixed, the strength domain given by Eq. (9) is a function of σ_z alone; hence, in view of Eqs. (13) and (3), $\bar{\tau}_{zy}$ turns out to be a function of two generalized strain only, *i.e.* $\bar{\tau}_{zy} = \bar{\tau}_{zy}(\varepsilon, \kappa)$.

Furthermore, it is a simple matter to verifiy that, for a fixed pair of values of ε and κ, $\bar{\tau}_{zy}$, depends on the y-coordinate with the same law of dependence on σ_z. Thus, the shear stress boundary $\bar{\tau}_{zy}(y)$ is still an ellipse over the beam cross-section, with center C and half major axis a equal to:

$$C \equiv \left(-\frac{\varepsilon}{\kappa} + \frac{2m\tau_o}{E\kappa}, 0\right) \qquad a = \frac{2\tau_o\sqrt{1+m^2}}{E\kappa} \qquad \textbf{(17)}$$

The intersections of the ellipse with the y-axis may or may not fall within the cross-section, depending on the values of ε, κ, in addition to those of the mechanical parameters E, m and τ_o, as shown by the following examples.

Lastly, from Eq. (16) and assuming for the sake of simplicity that the shear strain of each fiber is equal to an average value given by the generalized strain, *i.e.* $\gamma_{zy} = \gamma$, the shear stress τ_{zy} turn out to be a function of ε, κ and γ, *i.e.* $\tau_{zy} = \tau_{zy}(\varepsilon, \kappa, \gamma)$.

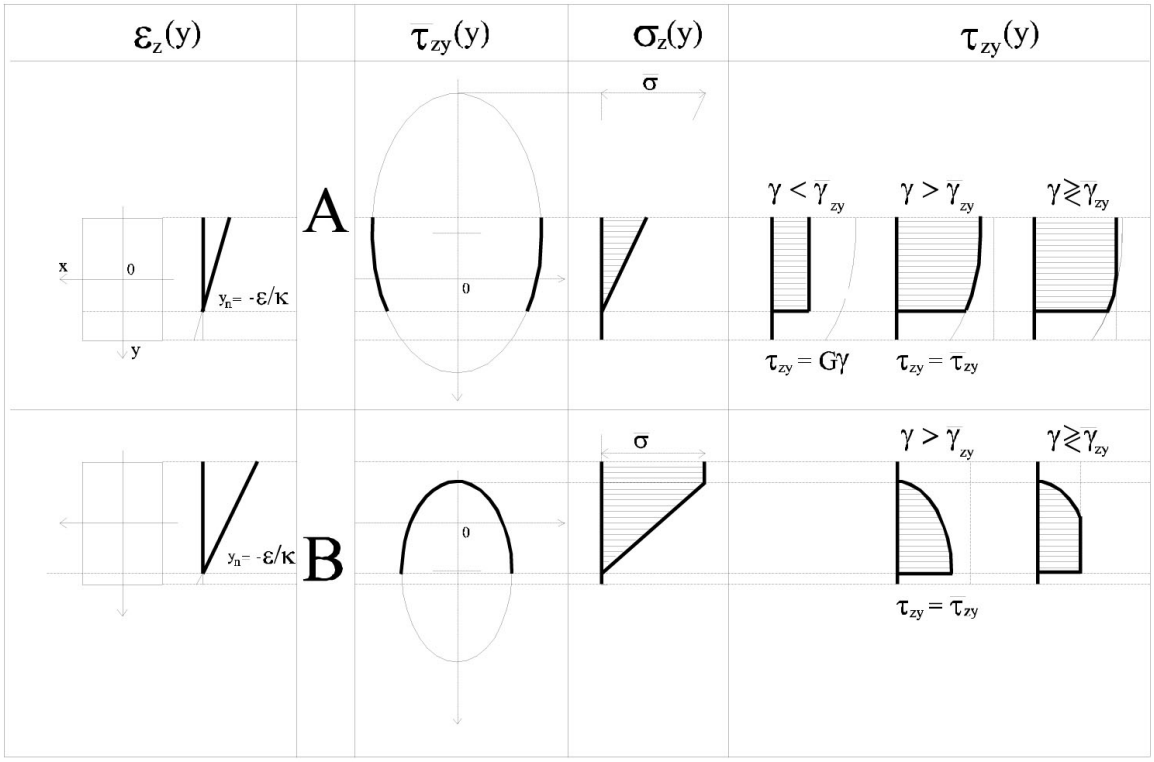

Fig. (8). σ_z and τ_{zy} patterns over a partialized beam cross-section.

Overall, many situations must be considered in order to define the patterns of the axial and tangential component σ_z and τ_{zy}, depending on the values of ε, κ and γ. Some of those deemed more significant are shown by way of example in the following.

With reference to a rectangular cross-section of dimensions b and $2h$, let us suppose that $\kappa > 0$ and the section is not partialized *i.e.* the ε_z pattern is the one shown in Fig. (**7**), where the neutral axis $y_n = -\varepsilon/\kappa$ does not cross the section.

In view of Eq. (17), the ordinate of the vertices of ellipse $\bar{\tau}_{zy}$ (y) must always be on the opposite sides with respect to y_n. Hence, in this case, with $y_n > h$, two qualitatively different circumstances can occurr depending on the values of ε and κ: both vertices of $\bar{\tau}_{zy}$ fall outside the section, or just one of them, as shown in Fig. (**7**) respectively in rows A and B, together with the corresponding σ_z pattern. Moreover, by simply comparing γ to $\bar{\gamma}_{zy}(y)$ of Eq. (15), any possible τ_{zy} pattern can also be obtained, as shown in the Fig. (**7**).

Essentially, different situations, leading to different τ_{zy} pattern, can occurr. With reference to the situation shown in row A of Fig. (**7**), it may turn out that $\gamma \leq \bar{\gamma}_{zy}(y)$ over the whole cross-section, *i.e.* for any $y \in [-h,h]$, so that $\tau_{zy}(y) = G\gamma$; or we can have $\gamma > \bar{\gamma}_{zy}(y)$ over the whole cross-section, and in this case $\tau_{zy}(y) = \bar{\tau}_{zy}(y)$; lastly, $\gamma > \bar{\gamma}_{zy}(y)$ may hold solely over a part of the section, with the consequent τ_{zy} pattern shown in Fig. (**7**). It is worth just noting that, in case of different positions of the ellipse with respect to the cross-section *i.e.* for various different values of of the strains (ε,κ)-, the latter situation ($\gamma \leqslant \bar{\gamma}_{zy}(y)$ for $y \in [-h,h]$) may provide further possible τ_{zy} pattern, not shown for the sake of brevity.

Similar situations can occur if the section is partialized, as shown in Fig. (**8**). Note that some situations, such as the entirely elastic case, are not consistent with the position of the ellipse and, thus, can not occurr.

Finally, once the σ_z and τ_{zy} patterns are known, for any value of (ε, κ, γ), the generalized stress -N, V and M are determined as

$$N = \int_A \sigma_z \, dA \qquad M = \int_A \sigma_z y \, dA \qquad V = \int_A \tau_{zy} \, dA \quad \textbf{(18)}$$

4. NUMERICAL RESULTS

The proposed model has been implemented into the finite element code MADY [12]. To obtain a locking-free Timoshenko beam element, only one Gauss point has been used for the numerical integration [28]. For the rest, the numerical procedure used is standard and has been described in detail elsewhere [12, 15, 16, 29], with reference to other types of "beam" elements.

To highlight the ability of the proposed beam model to capture the in-plane behaviour of masonry panels, some comparisons have been conducted with the numerical results obtained by means of two different 2D finite element models.

The first bi-dimensional model used has been developed by the authors themselves and is presented in detail in [26]. The model is an extension of the classical *masonry-like* or no-tension model [30, 31]: besides limiting the compressive strength, the model accounts, for a bound to the shear stress

component on each plane, that depends on the acting normal stress component. With reference to shear, the idea of the material constitutive behaviour is, therefore, the same used for developing the proposed beam model. Naturally, the two models differ essentially in the kinematic constraints and the consequent stress state given by Eq. 7. Moreover, they differ with regard to the hypothesis on the cohesive force acting on the cracked parts of the structure, being nil in the beam model but provided for the 2D model. The 2D model has been implemented into the code MADY and has been used in the following analyses with four-node elements in the plane stress framework.

The second model used a 2D model available within the FE commercial code ANSYS. Specifically, 2D geometries under the assumption of plane stress have been discretized by using PLANE182 finite elements, while the Mohr-Coulomb model with cut-off has been selected to represent the masonry's constitutive behavior [25].

It is also worth mentioning that the constitutive law of the two 2D models used are similar but not equivalent [32].

4.1. Comparisons for Single Panels

In this section, some comparisons with experimental results for a single panel are provided. Specifically, referring to the experimental research conducted at the Joint Research Centre in Ispra in 1995 [10, 24, 33 - 36], two geometries have been considered: A *squat panel* with 1.35 m height, and a *slender panel* with 2.0 m height, both of them having a rectangular cross-section 1 m in width and 0.25 m in thickness. As in the experimental tests, the panels are perfectly clamped at their base, with a further restraint to rotation at the top.

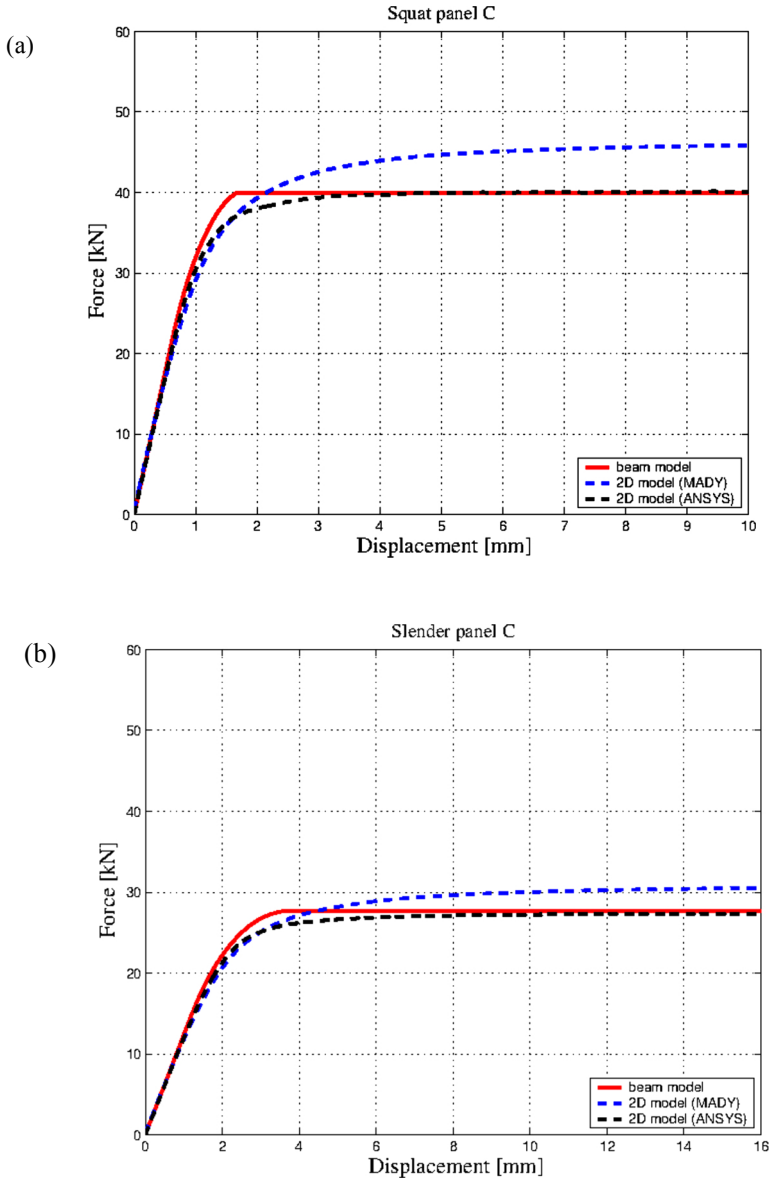

Fig. (9). Comparison with results from the 2D models for (**a**) the squat panel and (**b**) the slender panel.

Moreover, they have first been subjected to a constant vertical load P equal to $150kN$, which entails a normal compressive stress σ_z equal to $-0.6MPa$. The self-weight has also been considered, assuming for the mass density a value $\rho = 1800\ kg/m^3$ [24]. Then, all the analyses have been conducted by applying a monotonic increasing horizontal displacement at the top of the panels.

As per to some indications given in the literature [10, 24, 36], the main mechanical characteristics assumed are as follows: $E = 1800MPa$, $G = 820MPa$ ($i.e. \nu = 0.1$), $\sigma_o = -6.2MPa$, and for shear, the values $\tau_o = 0.72MPa$ and $m = -0.4$, have been chosen. It is worth noting that such values are reasonable, and fall within the range of values assumed in the aforementioned research papers to calibrate other numerical models. Naturally, the issue of assuming appropriate values for these material parameters is an open one, which requires comparisons with a large amount of experimental data, a task which is beyond the scope of the present paper.

For the numerical simulations, both panels have been discretized into 80 beam elements. The number of finite elements has been chosen to obtain the most accurate response provided by the model, also in view of the comparisons of the stress state given by the more refined 2D models. Decreasing the element number – down to very few elements, has shown to cause slight variations in the results – which are in any case conservative; conversely increasing the number of finite elements has not lead to any significant variation.

The global response of the analysed panels has been presented through pushover curves, *i.e.* shear force *vs* top displacement curves. Fig. (**9a**) shows the results obtained for the squat panel. The analogous diagrams for the slender panel are shown in Fig. (**9b**).

As shown in Figs. (**9a** and **b**), the responses obtained *via* the beam model are consistent with those from the 2D-models. Unsurprisingly, the response obtained *via* the beam model exhibits a slightly larger global stiffness with respect to that predicted through the 2D models. Nevertheless, the predicted total lateral strength of the panels are in very good agreement. It is quite interesting to note that no significant variation in the agreement of results emerges between the two structural cases considered, that is by varying the slenderness of the panels.

The accuracy of the beam model's predictions has been also verified from a local perspective. With reference to the squat case, Figs. (**10a** and **b**) provide a comparison with results obtained *via* the 2D models, respectively in terms of minimum principal stress σ_{min} - previously denoted by σ^- – and maximum shear stress τ_{max} attained throughout the panel. Such comparison is carried out at the loading step where a displacement of 5 mm is attained.

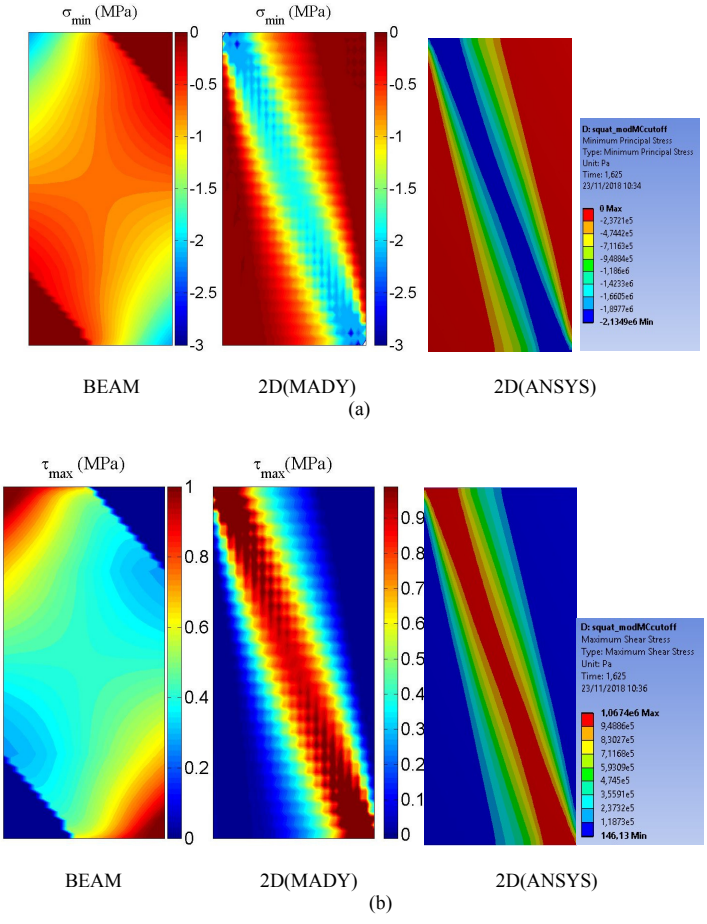

Fig. (10). Squat panel: Comparison of (**a**) σ_{min} and (**b**) τ_{max}.

As shown in Fig. (**10**), the beam model yields quite a different result in terms of stress state, despite the similar global response depicted in Fig. (**9**). The degree of stresses achieved at the top and the base of the panel provided by the beam model is acceptable, if compared with those predicted by the 2D models. However, the predicted stress state throughout the panel is more widespread if compared to that given by the two 2D models, which is confined to a limited area along the diagonal of the panel. Such a distribution cannot be captured by the beam model due to the embedded kinematic contraints.

Like the global responses, the local results for the slender panel are also qualitatively similar to the analogous ones shown in Fig. (**10**) for the squat case, and hence have not been presented here for the sake of brevity.

In the following, some further comparisons have been carried out by varying the boundary conditions, as they have proven to affect the panels response significantly.

Specifically, for each geometry, the following boundary conditions - widely assumed to represent the actual constraints in real buildings - have also been considered:

[i] the panels are perfectly constrained at the base and totally free at the top, a condition that in the following will be referred to as C, *i.e.* cantilever;

[ii] the panels, still clamped at their base, have further restraints on the axial displacement and rotation at the top nodes after application of the vertical load; such cases will be referred to as DF, which stands for double fixed.

Figs. (**11a** and **b**) show the pushover curves for the squat and the slender cantilevers (C panels), respectively. The trends of the results are similar to those already shown in Figs. (**9a** and **b**), thus confirming the ability of the simple model to provide an acceptable picture of the global response.

Fig. (**12**) shows the results obtained for the C slender panel in terms of stress state. In this case, contrary to what happens with the panel when top rotation is constrained, the proposed model appears to be more accurate in describing the state of stress in the panel body. Indeed, the stress state prediction is quite satisfactory if compared to that given by the 2D models. Results for the C squat panel are substantially similar and thus omitted here.

Fig. (**13**), where results analogous to those in Fig. (**11**) are illustrated for the DF panels, substantially confirms the previously revealed trends. The beam model provides an accurate prediction of the global response of the panel.

From a local point of view, trends qualitatively similar to Fig. (**10**) emerge from the DF panels stress state, not reported here.

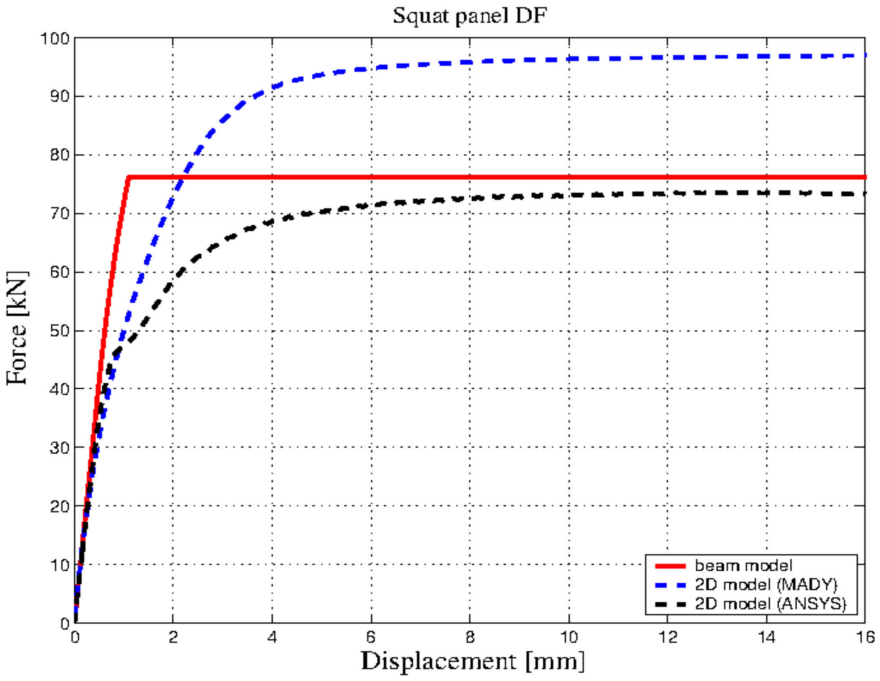

(a)

Fig. 11 contd.....

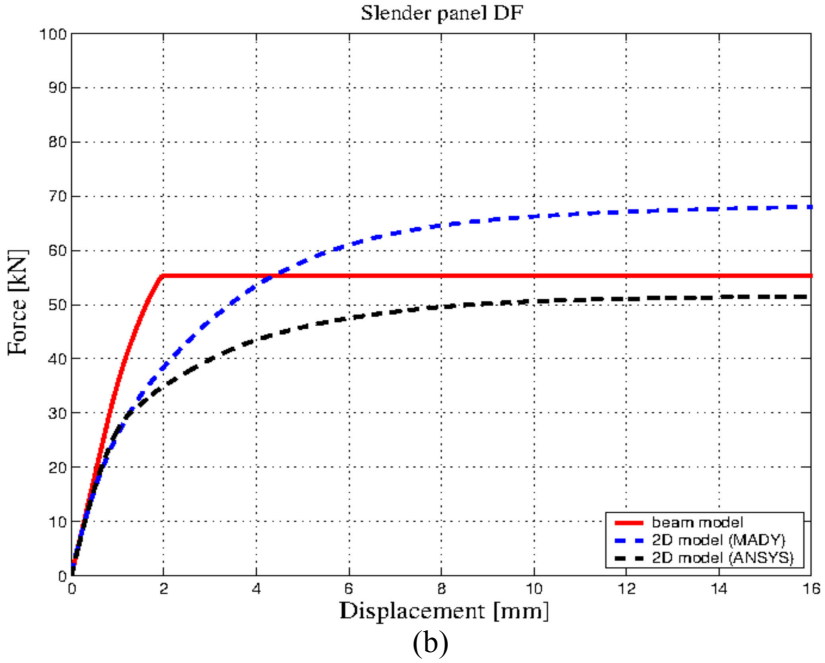

Fig. (11). C panel: pushover curves for (**a**) the squat and (**b**) the slender panel.

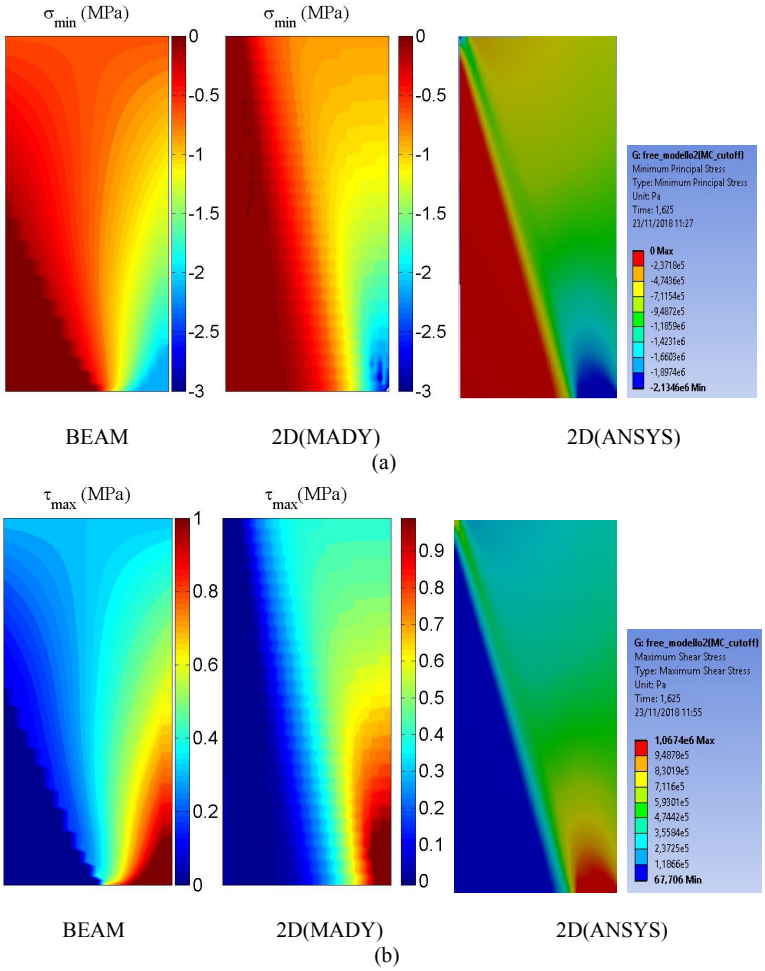

Fig. (12). C slender panel: comparison of (**a**) σ_{min} and (**b**) τ_{max}.

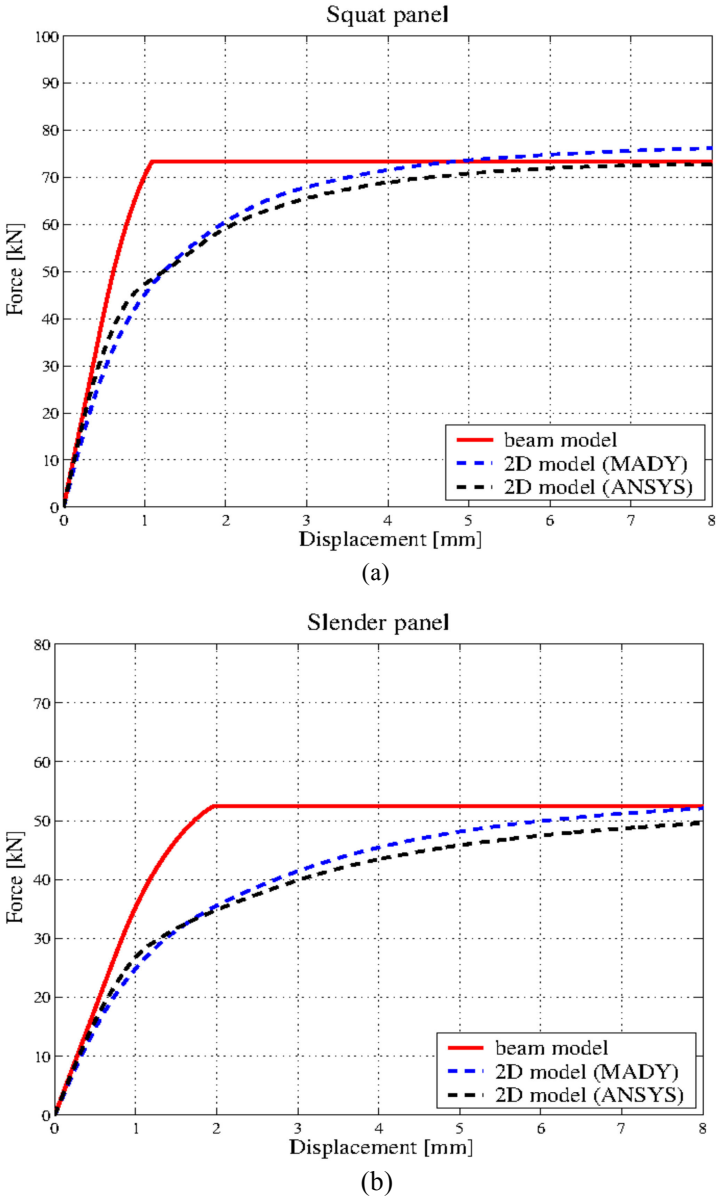

Fig. (13). DF panels: pushover curves for (**a**) the squat and (**b**) the slender panel.

4.2. A Wall with an Opening

Simplified models are especially useful for analyzing more complex structures than simple panels, for which sophisticated models may involve very high computational costs. Hence, in order to highlight the possible use of the proposed model in practical applications, some preliminary results are presented for an idealized masonry wall, provided for illustrative purposes only. In this framework, the wall is represented as an idealized frame, in which the piers and spandrels are connected through rigid offsets.

More in detail, the analysed structure is a wall with a centered opening (Fig. **14**). The wall's main geometrical characteristics are as follows: height = 3.2 m, width = 3.4 m and thickness = 0.25 m, while the dimensions of the opening are 2 x 1 m. As for the mechanical properties, the values used in the foregoing have been assumed, *i.e.* ρ = 1800kg/m^3, E = 1800MPa, v = 0.1, σ_o = -6.2MPa, and τ_o = -0.72MPa and m = -0.4.

In addition to the self-weight, a distributed vertical load - with total resultant of 220kN- is firstly applied at the top of the wall; then, it is subjected to an increasing horizontal displacement, keeping rotation at the top costrained.

A sketch of the idealized wall used in the finite element analysis is depicted in Fig. (**14**). The dimensions of the rigid nodes have been defined according to the relevant literature [2].

Using the proposed beam model, each pier has been modeled through 40 finite elements, while the spandrel has been discretized into 20 elements. Each node is instead represented by 6 (vertical) plus 6 (horizontal) rigid beam elements.

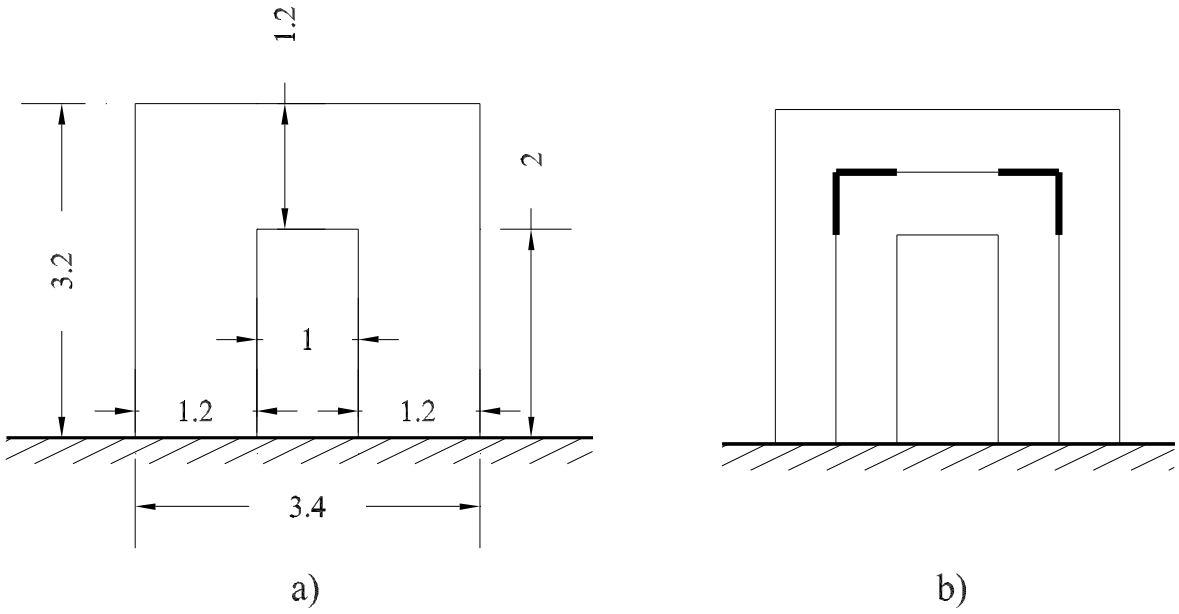

Fig. (14). The analyzed wall: geometry and beam model idealization.

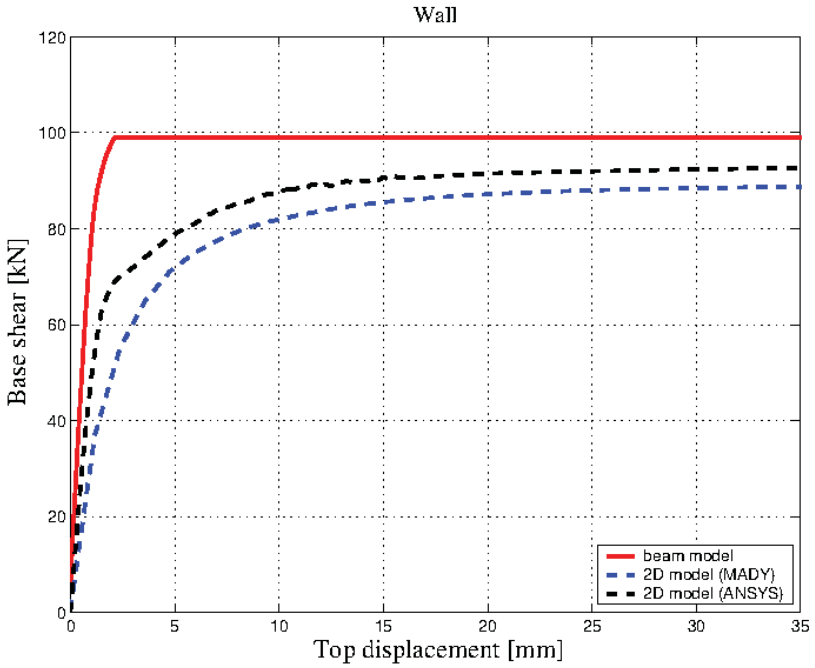

Fig. (15). Pushover curves of the wall: comparison of the beam model with 2D models.

The results have been compared with those obtained with the 2D models used in the foregoing, *i.e.* the masonry-like model implemented in MADY and the one available in ANSYS, assuming the same mechanical properties, load and constraint conditions.

Fig. (**15**), which shows the total base shear *vs* top displacement curves obtained *via* the three models, highlights a consistent trend with some slight difference in the total lateral capacity.

Obviously, although some promising results have been obtained, a number of issues still remain to be settled in order to enable using the proposed model for the analyses of real masonry structures, especially with regards to defining the behavior and geometries of the spandrels and rigid offsets.

CONCLUSION

The need to preserve an enormous heritage of masonry buildings, which as demonstrated by recent seismic events are extremely vulnerable to horizontal actions, calls for simplified models and low-computation numerical methods to perform preliminary and/or wide-area investigations.

It is to this end that a refined beam model has been

proposed. Starting with a no-tension material approach, the model has been enhanced by endowing it with the ability to describe shear behavior and predict the collapse mechanisms typically exhibited by relatively squat panels loaded in their plane.

Some comparisons with the results obtained through two different 2D models (which also account for a limit to shear stress) have been conducted to evaluate the accuracy of the results predicted by the proposed model. Despite its simplicity, the beam model is quite capable of capturing the panels global response. This is true regardless of the slender-ness and constraint conditions.

The model can also provide some broad indications on the local stress distribution in the panels. Also from a local perspective, the predictive capacity of the model is practically independent of the slenderness of the walls. Conversely, the accuracy of these results is affected by the panel's constraint conditions, being more acceptable for panels which are free at the top.

Lastly, some preliminary results have also been carried out for an idealized wall with an opening, in order to show the possible application of the proposed model to assess the seismic capacity of a masonry wall and facade through non-linear static analyses.

NOTATIONS

(o, y, z)	=	Reference system
b	=	Width of the beam's rectangular cross-section
$2h$	=	Height of the beam's rectangular cross-section
n	=	Normal unit vector
σ_n	=	Normal component of the stress
τ_n	=	Tangential component of the stress
T	=	Stress tensor
$\sigma_y, \sigma_z, \tau_{zy}$	=	Stress components
σ^-, σ^+	=	Principal stresses
$\varepsilon_y, \varepsilon_z, \gamma_{zy}$	=	Strain components
σ_o	=	Minimum compressive stress
τ_o	=	Cohesion
m	=	Internal friction
ρ	=	Density
E	=	Young's modulus
G	=	Stress tensor
v	=	Poisson's ratio
$\varepsilon, \kappa, \gamma$	=	Generalized strain
N, V, M	=	Generalized stress
u, v	=	Displacement component of the beam's axis
φ	=	Rotation of the cross-section

CONSENT FOR PUBLICATION

Not applicable.

CONFLICT OF INTEREST

The authors declare no conflict of interest, financial or otherwise.

ACKNOWLEDGEMENTS

Declared none.

REFERENCES

[1] M. Dolce, "Schematizzazione e modellazione degli edifici in muratura soggetti ad azioni sismiche", *L'Industria delle Costruzioni,* vol. 25, pp. 44-57, 1991.

[2] S. Bracchi, M. Rota, A. Penna, and G. Magenes, "Consideration of modelling uncertainties in the seismic assessment of masonry buildings by equivalent-frame approach", *Bull. Earthquake Eng.,* vol. 13, no. 11, pp. 3423-3448, 2015.

[3] C. Calderini, S. Cattari, and S. Lagomarsino, "In-plane strength of unreinforced masonry piers", *Earthquake Eng. Struct. Dynam.,* vol. 38, pp. 243-267, 2009. [http://dx.doi.org/10.1002/eqe.860]

[4] R. Marques, and P. Lourenço, "Possibilities and comparison of structural component models for the seismic assessment of modern unreinforced masonry buildings", *Comp. Struct.,* vol. 89, pp. 2079-2091, 2011. [http://dx.doi.org/10.1016/j.compstruc.2011.05.021]

[5] C.D. Ambra, G. Lignola, and A. Prota, "Multi-scale analysis of in-plane behaviour of tuff masonry", *Open Construct. Build. Technol. J,* vol. 89, pp. 312-328, 2016.(Suppl 2-M10)

[6] G. Magenes, and G. Calvi, "Prospettive per la calibrazione di metodi semplificati per l'analisi sismica di pareti murarie", *Atti del Convegno Nazionale La Meccanica delle murature tra teoria e progetto, Messina,* pp. 18-20, 1996. [in Italian]

[7] B. Calderoni, E. Cordasco, P. Lenza, and G. Pacella, "A simplified theoretical model for the evaluation of structural behaviour of masonry spandrels", *Int. J. Mat. Struct. Integr.,* vol. 5, pp. 192-214, 2011. [http://dx.doi.org/10.1504/IJMSI.2011.041934]

[8] R. Sabatino, and G. Rizzano, "A simplified approach for the seismic analysis of masonry structures", *Open Construct. Build. Technol. J.,* vol. 5, pp. 97-104, 2011.(Suppl 1-M7)

[9] S. Lagomarsino, A. Penna, A. Galasco, and S. Cattari, "TREMURI program: An equivalent frame model for the nonlinear seismic analysis of masonry buildings", *Eng. Struct.,* vol. 56, pp. 1787-1799, 2013. [http://dx.doi.org/10.1016/j.engstruct.2013.08.002]

[10] D. Addessi, A. Mastrandrea, and E. Sacco, "An equilibrated macro-element for nonlinear analysis of masonry structures", *Eng. Struct.,* vol. 70, pp. 82-93, 2014. [http://dx.doi.org/10.1016/j.engstruct.2014.03.034]

[11] E. Raka, E. Spacone, V. Sepe, and G. Camata, "Advanced frame element for seismic analysis of masonry structures: Model formulation and validation", *Earthquake Eng. Struct. Dynam.,* vol. 44, no. 14, pp. 2489-2506, 2015. [http://dx.doi.org/10.1002/eqe.2594]

[12] M. Lucchesi, and B. Pintucchi, "A numerical model for non-linear dynamics analysis of masonry slender structures", *Eur. J. Mech. A, Solids,* vol. 26, pp. 88-105, 2007. [http://dx.doi.org/10.1016/j.euromechsol.2006.02.005]

[13] N. Zani, "A constitutive equation and a closed-form solution for no-tension beams with limited compressive strength", *Eur. J. Mech. A, Solids,* vol. 23, no. 3, pp. 467-484, 2004. [http://dx.doi.org/10.1016/j.euromechsol.2004.01.008]

[14] M. Girardi, M. Lucchesi, C. Padovani, B. Pintucchi, G. Pasquinelli, and N. Zani, "Numerical methods for slender masonry structures: A comparative study", In: B.H.V. Topping, Ed., *Proceedings of the Eleventh International Conference on Computational Structures Technology - art. n.118,* Civil-Comp Press: Dubrovnik, Croatia, 2012, pp. 143-159.

[15] B. Pintucchi, and N. Zani, "A simple model for performing nonlinear static and dynamic analyses of unreinforced and FRP-strengthened masonry arches", *Eur. J. Mech. A, Solids,* vol. 59, pp. 210-231, 2016. [http://dx.doi.org/10.1016/j.euromechsol.2016.03.013]

[16] B. Pintucchi, and N. Zani, "Effects of material and geometric non-linearities on the collapse load of masonry arches", *Eur. J. Mech. A, Solids,* vol. 28, pp. 45-61, 2009.

[http://dx.doi.org/10.1016/j.euromechsol.2008.02.007]

[17] B. Pintucchi, and N. Zani, "Effectiveness of nonlinear static procedures for slender masonry towers", *Bull. Earthquake Eng.,* vol. 12, pp. 2531-2556, 2014.
[http://dx.doi.org/10.1007/s10518-014-9595-z]

[18] A. De Falco, and M. Lucchesi, "Stability of columns with no tension strength and bounded compressive strength and deformability. part i: large eccentricity", *Int. J. Solids Struct.,* vol. 39, pp. 6191-6210, 2002.
[http://dx.doi.org/10.1016/S0020-7683(02)00467-5]

[19] M. Lu, A. Schultz, H. Henryk, and K. Stolarski, "Application of the arc-length method for the stability analysis of solid unreinforced masonry walls under lateral loads", *Eng. Struct.,* vol. 27, no. 6, pp. 909-919, 2005.
[http://dx.doi.org/10.1016/j.engstruct.2004.11.018]

[20] M. Gurel, "Stability of slender masonry columns with circular cross-section under their own weight and eccentric vertical load", *Int. J. Archit. Herit,* vol. 10, no. 8, pp. 1008-1024, 2016.
[http://dx.doi.org/10.1016/j.engstruct.2009.12.005]

[21] I. Cancelliere, M. Imbimbo, and E. Sacco, "Experimental tests and numerical modeling of reinforced masonry arches", *Eng. Struct.,* vol. 32, pp. 776-792, 2010.
[http://dx.doi.org/10.1016/j.engstruct.2009.12.005]

[22] E. Grande, M. Imbimbo, and E. Sacco, "A beam finite element for nonlinear analysis of masonry elements with or without fiber-reinforced plastic (FRP) reinforcements", *Int. J. Archit. Herit.,* vol. 5, no. 6, pp. 693-716, 2011.
[http://dx.doi.org/10.1080/15583058.2010.490616]

[23] M. Valluzzi, M. Valdemarca, and C. Modena, "Behavior of brick masonry vaults strengthened by FRP laminates", *J. Compos. Constr.,* vol. 5, no. 3, pp. 163-169, 2001.
[http://dx.doi.org/10.1061/(ASCE)1090-0268(2001)5:3(163)]

[24] A. Penna, S. Lagomarsino, and A. Galasco, "A nonlinear macro-element model for the seismic analysis of masonry buildings", *Earthquake Eng. Struct. Dynam.,* vol. 43, pp. 159-179, 2014.
[http://dx.doi.org/10.1002/eqe.2335]

[25] A.N.S.Y.S., "Ansys [Computer software]", *ANSYS*. Canonsburg, PA.

[26] M. Lucchesi, B. Pintucchi, and N. Zani, "Masonry-like material with bounded shear stress", *Europe. J. Mech. Solid.,* vol. 72, pp. 329-340, 2018.
[http://dx.doi.org/10.1016/j.euromechsol.2018.05.001]

[27] D. Aita, R. Barsotti, and S. Bennati, "Notes on Limit and Nonlinear Elastic Analyses of Masonry Arches", In: D. Aita, O. Pedemonte, and K. Williams, Eds., *Masonry Structures: Between Mechanics and Architecture,* Birkhäuser: Cham, 2015, pp. 237-264.
[http://dx.doi.org/10.1007/978-3-319-13003-3_9]

[28] J. Reddy, "On locking free shear deformable beam elements", *Comput. Methods Appl. Mech. Eng.,* vol. 149, pp. 113-132, 1997.
[http://dx.doi.org/10.1016/S0045-7825(97)00075-3]

[29] M. Lucchesi, B. Pintucchi, M. Šilhavý, and N. Zani, "On the dynamics of viscous masonry beams", *Contin. Mech. Thermodyn.,* vol. 27, pp. 349-365, 2015.
[http://dx.doi.org/10.1007/s00161-014-0352-y]

[30] M. Lucchesi, C. Padovani, G. Pasquinelli, and N. Zani, "Masonry constructions: mechanical models and numerical applications", *Springer,* 2008.

[31] G. Del Piero, "Constitutive equations and compatibility of the external loads for linear elastic masonry-like materials", *Meccanica,* vol. 24, pp. 150-162, 1989.
[http://dx.doi.org/10.1007/BF01559418]

[32] M. Lucchesi, B. Pintucchi, and N. Zani, "Normal elastic and elastoplastic materials: a comprehensive approach", *Meccanica,* 2018.

[33] A. Anthoine, G. Magonette, and G. Magenes, "Shear-compression testing and analysis of brick masonry walls", In: *Proc. of the 10th European Conference on Earthquake Engineering, Duma Ed,* 1995, pp. 1657-1662.

[34] G. Magenes, and G.M. Calvi, "In-plane seismic response of brick masonry walls", *Earthquake Eng. Struct. Dynam.,* vol. 26, pp. 1091-1112, 1997.
[http://dx.doi.org/10.1002/(SICI)1096-9845(199711)26:11<1091::AID-EQE693>3.0.CO;2-6]

[35] L. Gambarotta, and S. Lagomarsino, "Damage models for the seismic response of brick masonry shear walls. part II: the continuum model and its applications", *Earthquake Eng. Struct. Dynam.,* vol. 26, pp. 441-462, 1997.
[http://dx.doi.org/10.1002/(SICI)1096-9845(199704)26:4<441::AID-EQE651>3.0.CO;2-0]

[36] C. Calderini, and S. Lagomarsino, "Continuum model for in-plane anisotropic inelastic behaviour of masonry", *J. Struct. Eng.,* vol. 134, no. 2, pp. 209-220, 2008.
[http://dx.doi.org/10.1061/(ASCE)0733-9445(2008)134:2(209)]